INTERNATIONAL JOURNAL FOR NUMERICAL METHODS IN FLUIDS
Int. J. Numer. Meth. Fluids 2010; **63**:163–184
Published online 29 December 2009 in Wiley InterScience (www.interscience.wiley.com). DOI: 10.1002/fld.2219

Equation-free model reduction for complex dynamical systems

O. P. Le Maître[1, 2, *, †] and L. Mathelin[1]

[1]*LIMSI-CNRS, BP 133, 91403 Orsay, France*
[2]*CEA/DM2S/SFME, Centre d'Etudes de Saclay, France*

SUMMARY

This paper presents a reduced model strategy for simulation of complex physical systems. A classical reduced basis is first constructed relying on proper orthogonal decomposition of the system. Then, unlike the alternative approaches, such as Galerkin projection schemes for instance, an equation-free reduced model is constructed. It consists in the determination of an explicit transformation, or mapping, for the evolution over a coarse time-step of the projection coefficients of the system state on the reduced basis. The mapping is expressed as an explicit polynomial transformation of the projection coefficients and is computed once and for all in a pre-processing stage using the detailed model equation of the system. The reduced system can then be advanced in time by successive applications of the mapping. The CPU cost of the method lies essentially in the mapping approximation which is performed offline, in a parallel fashion, and only once. Subsequent application of the mapping to perform a time-integration is carried out at a low cost thanks to its explicit character.

Application of the method is considered for the 2-D flow around a circular cylinder. We investigate the effectiveness of the reduced model in rendering the dynamics for both asymptotic state and transient stages. It is shown that the method leads to a stable and accurate time-integration for only a fraction of the cost of a detailed simulation, provided that the mapping is properly approximated and the reduced basis remains relevant for the dynamics investigated. Copyright © 2009 John Wiley & Sons, Ltd.

Received 25 November 2008; Revised 24 July 2009; Accepted 11 August 2009

KEY WORDS: model reduction; POD; equation-free model; coarse time-step; Navier–Stokes equations

1. INTRODUCTION

Simulation of complex multiscale and multiphysics systems remains a challenge as the size of discrete problems is often an issue. Examples of complex multiscale systems can be found in many engineering fields, such as in tribology (quantum mechanics effects), fluid mechanics (turbulent flow), and combustion (complex reaction mechanisms involving thousands of species and reactions

*Correspondence to: O. P. Le Maître, LIMSI-CNRS, BP 133, 91403 Orsay, France.
†E-mail: olm@limsi.fr

Contract/grant sponsor: ANR; contract/grant number: ANR-08-JCJC-0022

over multiple order of time-scales). These systems leave us with a large number of degrees of freedom to be considered and, even with the growing computational power, such problems remain intractable as such. However, most often, one is not interested in the detailed solution but rather in some macroscopic quantities, such as integral or time-average quantities, characteristic of only the most salient and essential features of the system, disregarding the details of secondary importance. Often, these quantities of interest have a dynamics that exists in a much lower-dimensional space compared with the actual system, suggesting that they can be predicted using a much lighter model involving a significantly lower number of degrees of freedom than for the detailed one. This observation has raised the need for efficient model reduction procedures, which are of utmost importance in optimization and control problems where simulations are to be performed at a minimum cost or in a real-time context.

Many different model reduction strategies have been proposed in the literature, the best of which often being case-dependent. For instance, if the underlying difficulty of the detailed simulation lies in the wide range of scales, scales separation strategies that decouple phenomena at different scales may be appropriate. An example of scales separation treatment is the Large Eddy Simulation, where the effects of subgrid scale flow dynamics onto large-scale turbulent structures are modelled (see [1]). Similarly, chemical systems often involve a set of reactions whose kinetics may be several orders of magnitude apart. One popular approach is then to identify slow and fast manifolds onto which the system dynamics may be decoupled and the solution approximated (see [2]). Another reduction approach consists in restricting the approximated solution to live in the subspace spanned by its first principal components, i.e. generated by the first eigenvectors of its covariance operator. This is the widely used Karhunen–Loeve (KL) approach also termed the proper orthogonal decomposition (POD) in the fluid mechanics community.

Here, we adopt the latter type of reduction approach, where a time–space dependent variable u is reduced in the series $u(\boldsymbol{x},t)\simeq\overline{u}(\boldsymbol{x})+\sum_m a_m(t)\Omega_m(\boldsymbol{x})$ with $\overline{u}(\boldsymbol{x})$ the time-average of $u(\boldsymbol{x},t)$. In practice, the series is truncated to a (low) finite number M of terms. From this series, one has to derive a model for the temporal evolution of the reduced model coefficients $a_m(t)$, $m=1,\ldots,M$. A common procedure consists in inserting the series into the original model equations and to require the resulting equations residual to be orthogonal to the sub-space spanned by the M modes Ω_m, in a prescribed inner product sense. This is the Galerkin projection method. It results in a set of M coupled ordinary differential equations (ODEs) for the temporal coefficients $a_m(t)$ of the M modes retained in the model reduction. However, the resulting reduced model will generally not mimic exactly the dynamics of the detailed model, as the contribution of the disregarded modes on the dynamics is removed. In fact, although the neglected modes may have a negligible contribution to the series expansion of u, they can have a significant impact on the dynamics: the reduced and original systems may have different attractors. As a result, simulation of the reduced system derived by Galerkin projection usually exhibits a slow drift of the trajectory in the phase space from the actual attractor. The larger the M, the slower the drift. Further, neglected modes often correspond to shorter physical scale contributions to the solution and are mostly responsible for energy dissipation. The approximation given by a truncated series thus lacks dissipative scales and the resulting time-integration of the reduced system can be unstable. To address this issue, different treatments have been proposed in the literature, most of them based on the introduction of correction terms in the reduced model equations for the a_m, e.g. viscous and non-linear damping terms (see for instance [3–5]) or determined by calibration techniques [6–8].

An alternative approach to the Galerkin projection consists in determining the reduced model for the coefficients evolution through a non-linear regression or a learning procedure. The reduced

DOI: 10.1002/fld

model form is prescribed, possibly based on physical considerations, and the model parameters are identified using detailed model simulations or observations of the flow. Recent works provide examples of such an approach (see, for instance, a neural network [9]). One of the main limitations of this type of reduced model construction is that its robustness against conditions different from those used during the identification process remains an essentially unresolved issue.

In this work, we resort to an equation-free approach where one does not look for an evolution equation for the coefficients in closed form but rather tries to directly approximate the explicit transformation of the set of reduced model coefficients $a_m(t)$ as time advances. This procedure presents the advantage to bypass the need for the *a priori* prescription of a particular model form. As a result, the approximation does not take place at the design stage of the reduced model, but instead when determining the transformation that relates the reduced coefficients set, after some time elapsed, to their current values. Adopting such a point of view, one expects to obtain more general and robust reduced models able to mimic a broader range of dynamics. This is of critical importance if one wants the whole reduction strategy to be of any general relevance. Indeed, reduced models are to be used to predict the dynamics of a system in conditions which usually differ from the one used for deriving it. As mentioned above, this is essential in view of using the reduced models to derive control strategies for the system. In that case, the system dynamics will be affected by the control action and the reduced model has to preserve its predictive capability for those modified dynamics to be useful. In the present approach, this is achieved by approximating the evolution of the reduced model coefficients over an entire domain in the phase space, and not by a fitting procedure with some particular dynamics. In addition, the transformation (or mapping) of the reduced model coefficients is sought over a coarse time-step as a polynomial form, in a pre-processing stage, a convenient format that makes successive applications of the mapping a computationally inexpensive task.

The outline of the paper is as follows. In Section 2, we introduce the physical model and governing equations for the test system used throughout the paper. The system considered is the flow around in a 2-D circular cylinder in laminar regime. In Section 3, the size of the problem is first reduced by considering only the most representative, in the ergodic sense, modes of the flow; these modes are determined by means of the POD method that is described and finally applied to the test system, yielding the reduced basis representation. The construction of the reduced model is then considered in Section 4. The ideas of equation-free model and coarse time-integration are first recalled to motivate the representation of the dynamics by means of an explicit transformation of the coefficients of the system state on the reduced basis. Then, the methodology for the approximation of the mapping by a polynomial transformation is introduced. Application of the reduced model to the flow around the cylinder is considered in Section 5. The efficiency of the reduced model and the effect of its different parameters on the resulting predictions are investigated for both asymptotic and transient regimes. Finally, concluding remarks and perspectives are proposed in Section 6.

2. DETAILED FLOW MODEL

We consider the two-dimensional flow around a circular cylinder, with diameter R and centered on the origin, in an infinite domain. The inflow is uniform with velocity U_∞ along the x-axis of the space. The fluid is assumed to be incompressible and Newtonian with density ρ and viscosity μ. The governing equations are then the incompressible Navier–Stokes equations. The flow regime is a function of the characteristic Reynolds number $Re \equiv \rho U_\infty R/\mu$. In the detailed flow model, the

DOI: 10.1002/fld

dimensionless Navier–Stokes equations are time integrated in vorticity stream-function formulation. These equations are [10]:

$$\frac{\partial \omega}{\partial t} + \boldsymbol{u} \cdot \nabla \omega = \frac{1}{Re} \nabla^2 \omega, \tag{1a}$$

$$\nabla^2 \psi = -\omega, \tag{1b}$$

$$\boldsymbol{u} = \nabla \wedge (\psi \boldsymbol{k}), \tag{1c}$$

$$\omega \boldsymbol{k} = \nabla \wedge \boldsymbol{u}, \tag{1d}$$

where ω is the vorticity field, $\boldsymbol{u}$ is the velocity field, and ψ is the stream-function. We have also denoted $\boldsymbol{k}$ as the direction normal to the flow plane. Boundary conditions for the flow are no-slip velocity ($\boldsymbol{u} = 0$) on the cylinder surface, and undisturbed flow velocity at infinity. The equations are solved in a finite domain Ω, bounded internally by the cylinder surface γ_R and externally by the circle γ_∞ defined by $\|\boldsymbol{x}\| = R_\infty \gg R$ (Figure 1). Boundary conditions for ω and ψ are required for the resolution of Equation (1). On γ_∞, we set $\psi = \psi_\infty$ where ψ_∞ is the stream-function of the undisturbed flow, and we use homogeneous Dirichlet or natural out-flow boundary conditions for ω depending on the sign of the normal velocity:

$$\begin{aligned} &\omega(\boldsymbol{x}) = 0 \quad \forall \boldsymbol{x} \in \gamma_\infty | \boldsymbol{u} \cdot \boldsymbol{n} \geqslant 0, \\ &\frac{\partial \omega}{\partial t} = -\boldsymbol{u} \cdot \nabla \omega \quad \forall \boldsymbol{x} \in \gamma_\infty | \boldsymbol{u} \cdot \boldsymbol{n} < 0. \end{aligned} \tag{2}$$

On the cylinder, the values of ω and ψ (constant over the γ_R) are determined by means of influence matrix techniques [11].

The computations presented in the following use $R_\infty = 30$. The physical domain is conformally mapped to the rectangular domain $(X, Y) \in [0, 2] \times [0, 2\pi]$ discretized using a uniform grid consisting of 180×180 points. Then, the detailed model possesses 180^2 degrees of freedom.

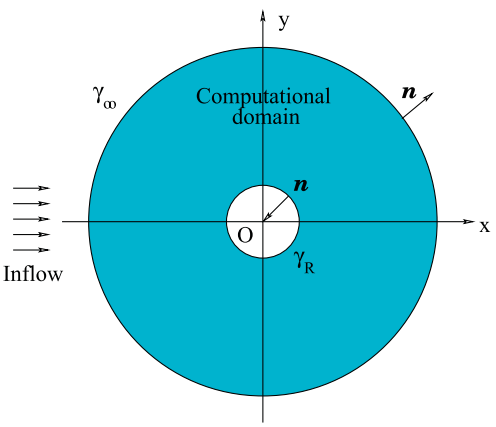

Figure 1. Sketch of the computational domain for the flow around the cylinder. The inflow velocity is uniform, and the computational domain has two boundaries: the cylinder surface γ_R and the far-field boundary γ_∞.

DOI: 10.1002/fld

Classical second-order finite difference schemes are used for the spatial discretization of the operators. The conformal transformation allows for fast (FFT-based) inversion of the Laplacian and diffusion operators. A second-order time discretization is employed to integrate the discrete problem. We classically rely on an explicit treatment of the non-linear (convective) term and an implicit treatment of the linear (diffusion) one. Overall, the integration over one time-step involves the resolution of 2 Helmholtz and 2 Poisson equations. More details about the flow solver and discretization may be found in [12].

3. REDUCED BASIS CONSTRUCTION

We have seen that the detailed model has 180^2 degrees of freedom after discretization. However, the flow dynamics lives in a much lower-dimensional space. This observation motivates the projection of the system on a low-dimensional manifold, with dimension $M \ll 180^2$, preserving the essential characteristics of its dynamics. This requires the determination of a reduced basis for the manifold.

In this work, we considered the Proper Orthogonal Decomposition (POD or Karhunen–Loève-KL-decomposition) [13, 14], as this decomposition is the most often used in the literature. However, we stress that the mapping strategy for the integration of the reduced model, to be introduced later, extends immediately to any orthogonal basis. In this section, we recall the essential theory and main properties of the POD and its practical determination which is finally applied to the flow around the cylinder.

3.1. Proper orthogonal decomposition

Basically, we are looking for a projection of the time-dependent vorticity field $\omega(\boldsymbol{x}, t)$ onto a low-dimensional basis $\{\Omega_0(\boldsymbol{x}), \ldots, \Omega_M(\boldsymbol{x})\}$:

$$\omega(\boldsymbol{x}, t) \approx \Omega(\boldsymbol{x}, t) \equiv \sum_{m=0}^{M} a_m(t)\Omega_m(\boldsymbol{x}). \tag{3}$$

In this expansion, the $\Omega_m(\boldsymbol{x})$ are the spatial modes of the flow, while the $a_m(t)$ are the time-dependent coefficients. The objective is to construct a basis that minimizes in some sense the distance (or truncation error) between the actual (ω) and projected (Ω) vorticity fields. This requires a definition of the projection error, ε, which is classically taken as the mean-square distance:

$$\varepsilon^2 \equiv \left\langle \left[\int\int (\omega(\boldsymbol{x}, t) - \Omega(\boldsymbol{x}, t))^2 \, \mathrm{d}\boldsymbol{x} \right] \right\rangle_t, \tag{4}$$

where we have denoted $\langle \cdot \rangle_t$ the time-averaging operator:

$$\langle f \rangle_t \equiv \lim_{T \to \infty} \frac{1}{T} \int_0^T f(t) \, \mathrm{d}t.$$

Considerations on the convergence of ε to 0, for increasing M, provide the means for the determination of the basis. An optimal choice, with regard to the error ε, is obtained when the basis functions Ω_m are the eigenfunctions of the spatial correlation function of the vorticity field.

The starting point of the POD is the separation of $\omega(\boldsymbol{x}, t)$ in time averaged and fluctuating components:

$$\omega(\boldsymbol{x}, t) = \overline{\omega}(\boldsymbol{x}) + \omega'(\boldsymbol{x}, t), \quad \langle \omega'(\boldsymbol{x}, t) \rangle_t = 0. \tag{5}$$

DOI: 10.1002/fld

Let $C_\omega(\boldsymbol{x},\boldsymbol{y})$ be the two-point correlation function of the fluctuation field:

$$C_\omega(\boldsymbol{x},\boldsymbol{y}) \equiv \langle \omega'(\boldsymbol{x})\omega'(\boldsymbol{y})\rangle_t. \tag{6}$$

The spatial mode $\Omega_m(\boldsymbol{x})$ and its associated non-negative, real, coefficient λ_m solves the following Fredholm integral equation (or eigen problem):

$$\iint C_\omega(\boldsymbol{x},\boldsymbol{y})\Omega_m(\boldsymbol{y})\,\mathrm{d}\boldsymbol{y} = \lambda_m \Omega_m(\boldsymbol{x}) \tag{7}$$

and, since $C_\omega(\boldsymbol{x},\boldsymbol{y})$ is real-valued and symmetric, the modes Ω_m are mutually orthogonal.

The spectral coefficients $a_{m\geqslant 1}(t)$ are finally given by

$$a_m(t) = \iint (\omega(\boldsymbol{x},t) - \langle\omega\rangle_t(\boldsymbol{x}))\Omega_m(\boldsymbol{x})\,\mathrm{d}\boldsymbol{x} \tag{8}$$

and are mutually orthogonal:

$$\langle a_l(t)a_m(t)\rangle_t = \lambda_m \delta_{lm}. \tag{9}$$

3.2. Practical determination of POD

The computation of the POD of ω' using the eigenvalue problem equation (7) is difficult in practice because of the size of its discretized version. Indeed, for the discretization of the flow introduced previously, the size of the discrete modes is 180^2. Of course, as the spectrum of C_ω is expected to be limited, only the first M dominant eigenvalues are to be computed, allowing for efficient computational strategy. Still, the full correlation kernel, has to be built and stored, raising computational and memory requirement issues. To overcome this difficulty, an alternative approach has been proposed. It takes advantage of the bi-orthogonality of the POD to develop a construction method based on the spectral decomposition of the time correlation kernel. This technique is referred to as the Snapshots method in the literature [15].

Let $\{\omega'^i(\boldsymbol{x}) \equiv \omega'(\boldsymbol{x},t_i)\}$, $i=1,\ldots,S$ be a finite sample set of the fluctuating field, and denote $C_{i,j}$ the $S\times S$ real matrix defined as:

$$C_{i,j} = \iint \omega'^i(\boldsymbol{x})\omega'^j(\boldsymbol{x})\,\mathrm{d}\boldsymbol{x}. \tag{10}$$

The matrix $C_{i,j}$ is symmetric and positive. Let us denote $\lambda_1 \geqslant \lambda_2, \ldots, \geqslant \lambda_{M\leqslant S}$ be the dominant eigenvalues of $C_{i,j}$ with associated normalized discrete eigenfunctions $a_1^{\mathrm{T}}(\cdot), a_2^{\mathrm{T}}(\cdot), \ldots, a_M^{\mathrm{T}}(\cdot)$. The POD modes of the fluctuating vorticity field can be expressed as:

$$\Omega_m(\boldsymbol{x}) = \sum_{i=1}^{S} \sqrt{\lambda_m} a_m^{\mathrm{T}}(t_i)\omega'^i(\boldsymbol{x}), \quad m=1,\ldots,M. \tag{11}$$

Compared with the decomposition of the spatial correlation kernel, the Snapshot method requires much less computational and memory effort, because the number of samples S needed for an accurate determination of the dominant modes is much lower than the number of degrees of freedom of the detailed model (180^2). Note also that for the Reynolds numbers considered in this paper, one has interest in taking advantage of the time-periodicity of flow, taking uniformly distributed snapshots on a single period of the flow.

DOI: 10.1002/fld

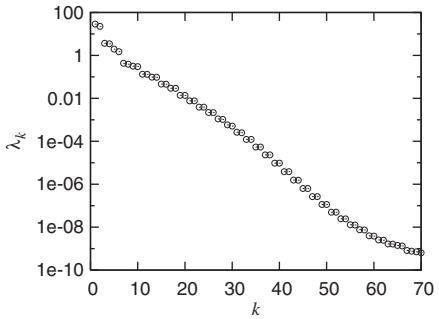

Figure 2. POD spectrum (from 128 snapshots) for the flow around the cylinder at $Re = 200$.

3.3. Application to the flow around a cylinder

The POD decomposition of the flow around the cylinder is now performed for $Re = 200$.

Figure 2 shows the truncated spectrum (λ_m) of $C_{i,j}$ for a sample set with dimension $S = 256$ of evenly distributed snapshots. The fast decay of the spectrum demonstrates the fast convergence of the POD of the vorticity field, hence, the truncation of the POD to the first $M \simeq 20$ modes captures essentially all of the vorticity fluctuations.

We now focus on the spatial structure of the first 12 POD modes $\Omega_m(\boldsymbol{x})$ depicted in Figure 3. The first two modes present an alternate pattern of positive and negative vorticity values extending far downstream of the cylinder (the flow goes from left to right); the characteristic length scale in fact corresponds to the von Kármán street which is indeed the dominant feature of the flow. Modes 3 and 4 also appear to mainly contribute to the representation of the von Kármán street, although they contain higher spatial frequencies (twice as high). Subsequent modes are more localized, essentially concentrated in the immediate vicinity of the cylinder and featuring high spatial frequencies, i.e. details at smaller scales. They account for more subtle details of the flow field.

Focusing now on the temporal evolution of the POD modes, the first coefficients $a_i(t)$ are plotted during one period of the flow in Figure 4 (Left) for the even index modes and (Right) for the odd index modes. Their corresponding frequency spectra are shown in Figure 5 (Left) and (Right), respectively. The first modes, accounting for the von Kármán street, are seen to evolve in a slow, large amplitude, manner. In fact, the first two modes exactly have the Strouhal or natural frequency of the wake (≈ 0.11) and are in phase opposition. The following modes have decreasing energy and fundamental frequency increasing with the mode index. It confirms that higher-order modes account for short-scale details of the vorticity field and carry less and less energy as the mode index increases.

4. CONSTRUCTION OF A REDUCED MODEL

4.1. Equation-free model—coarse time-stepping

The reduced basis for the flow being constructed, we focus now on the construction of a reduced model approaching the flow dynamics. Classically, reduced models are based on a set of evolution equations (ODEs) for the temporal coefficients $a_m(t)$. These equations aim at describing the dynamics of the detailed model (i.e. the detailed CFD model resulting from the discretization of

DOI: 10.1002/fld

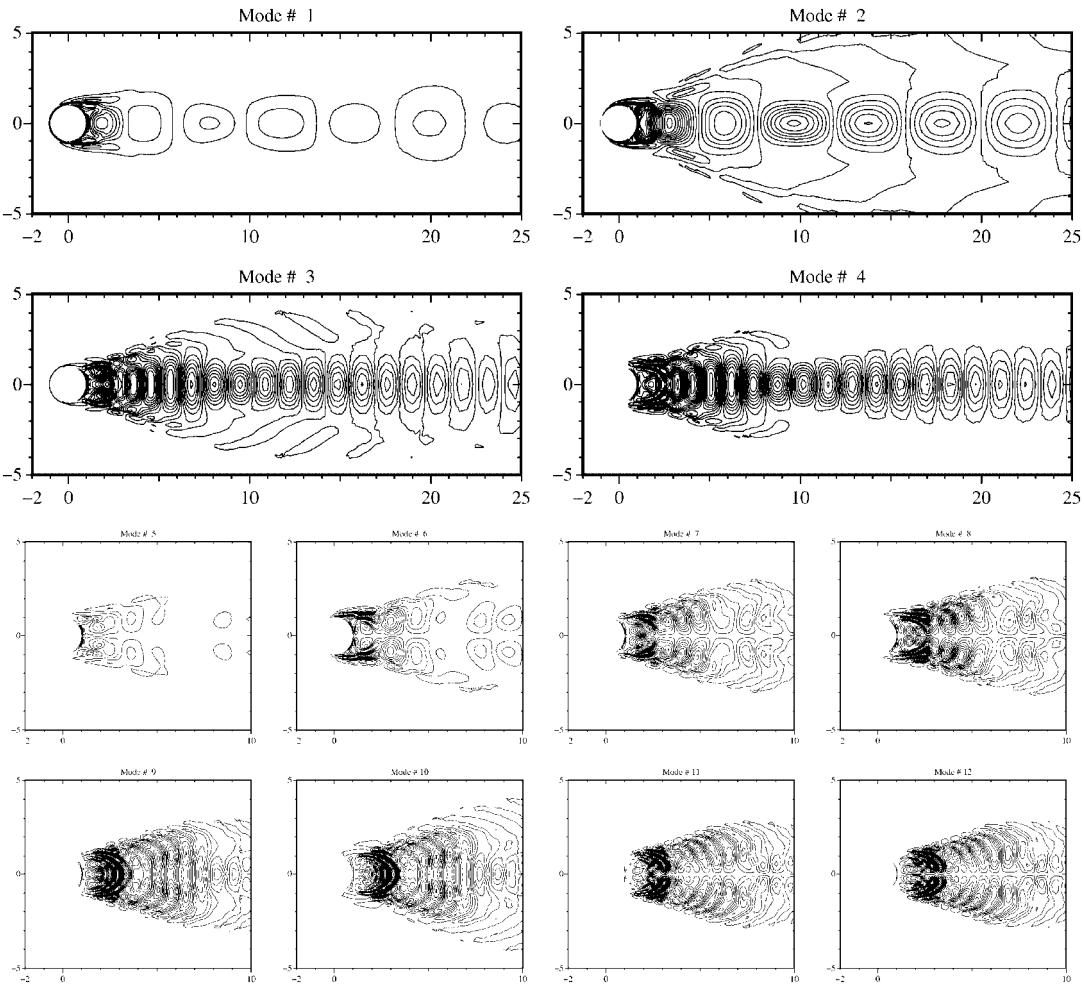

Figure 3. Spatial structure of the first 12 POD modes of the flow field at $Re = 200$.

the Navier–Stokes equations) in the reduced space spanned by the modes $\Omega_m(\boldsymbol{x})$. Often, equations for the dynamics in the reduced space are determined by means of Galerkin projection of the detailed model equations on the reduced basis.

The Galerkin technique therefore provides a set of governing equations for the temporal coefficients of the reduced model. Alternatively, one can derive the so-called equation-free methods to integrate in time the evolution of the coefficients $a_m(t)$, $m < M$ [16, 17]. These methods are said to be equation free as they do not rely on explicit equations for the integration of the $a_m(t)$, but instead use the detailed model (here the Navier–Stokes solver) to estimate their rate of change. The main assumptions supporting equation-free methods are: first, the relevance of reduced basis to properly represent the system's state and second, the scale-separation between the dynamics of the reduced modes ($\leqslant M$) and the truncated ones ($> M$). The scale-separation means that modes with index $> M$ are somehow slaved to reduced model modes ($m \leqslant M$): the dynamics of $a_{m>M}$ is

DOI: 10.1002/fld

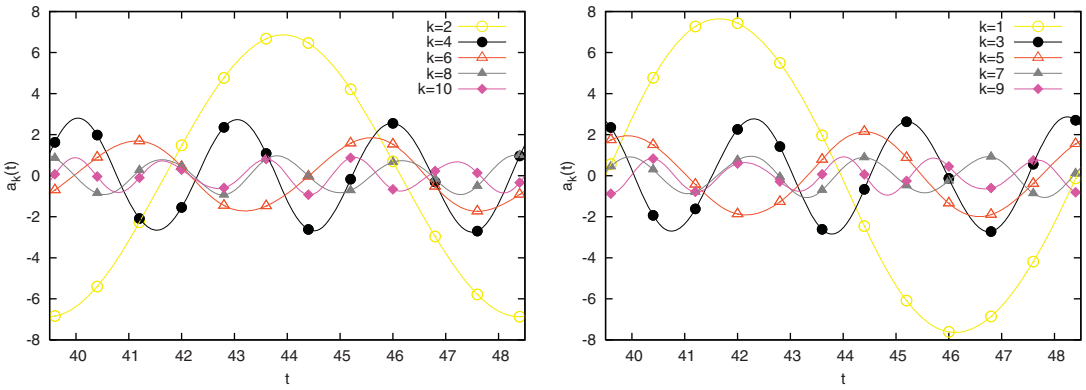

Figure 4. Example of time-evolution of the first 10 POD temporal coefficients $a_k(t)$ over a period of the flow around the cylinder. Left: even index modes; right: odd index modes.

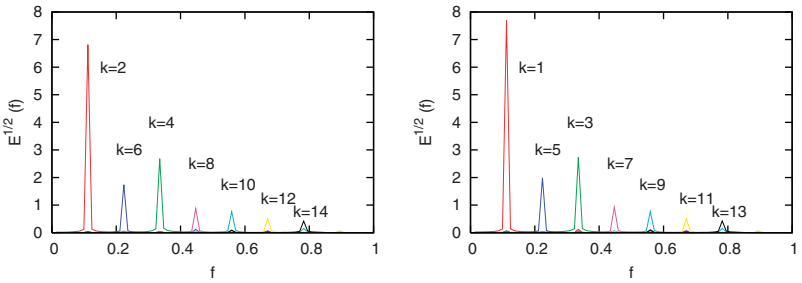

Figure 5. Frequency spectrum of the first 12 POD temporal coefficients $a_k(t)$ for the flow around the cylinder at $Re=200$. Left: even index modes; right: odd index modes.

essentially governed by $a_{1\leqslant m\leqslant M}$. Then starting at t_0 from an arbitrary initial state, we assume that within a short time-span τ, the system reaches an equilibrium where we have

$$a_{m>M}(t>t_0+\tau)\approx h_{m>M}(a_1(t),\ldots,a_M(t)). \tag{12}$$

As a result, starting from an initial truncated state, $\omega(\boldsymbol{x},t)=\sum_{m=0}^{M}a_m(t)\Omega_m(\boldsymbol{x})$, after a short period of time, say τ, the system reaches a state $\omega(\boldsymbol{x},t+\tau)=\sum_{m=0}^{M}a_m(t+\tau)\Omega_m(\boldsymbol{x})+\omega''(\boldsymbol{x},\tau)$, where the dynamics of ω'' is governed by the reduced modes.

Then, assuming that the relaxation time τ is short compared with characteristic time-scales of the reduced modes dynamics, one can estimate the instantaneous rates of change for the temporal coefficients, $\dot{a}_m\equiv \mathrm{d}a_m/\mathrm{d}t$, by classical finite differences and use these estimates to integrate the $a_m(t)$ with a coarse time-step T longer than τ. This leads to the following equation-free integration scheme:

1. Set the system state at time t,

$$\omega(\boldsymbol{x},t)=\sum_{m=0}^{M}a_m(t)\Omega_m(\boldsymbol{x}). \tag{13}$$

2. Run the detailed model for a small time-interval τ.

DOI: 10.1002/fld

3. Project the detailed solution at $t+\tau$ on the reduced basis: $a_m(t+\tau)$.
4. Estimate rates of change $\dot{a}_m$ at time t from $a_m(t)$ and $a_m(t+\tau)$.
5. Advance in time the coefficients a_m, from t to $t+T$, with $T>\tau$ using estimates $\dot{a}_m$.
6. Update time, $t \leftarrow t+T$, and repeat from step 1.

It is remarked that the initialization step could also include a contribution of the truncated modes, e.g. by randomly selecting $a_{m>M}(t)$, as they are supposed to quickly reach an equilibrium state with regards to the reduced ones. In any case, it is important to note that the initialization from any linear combination of $\Omega_m(\boldsymbol{x})$ yields a vorticity field that satisfy the problem boundary conditions.

Different integration techniques can be used for the time-integration of the coefficients a_m, ranging from the simplest Euler to advanced Runge–Kutta schemes. However, multi-step integrations require multiple estimates for the $\dot{a}_m$ along the coarse time-step T, and so multiple runs of the detailed model. Computational savings in equation-free methods are achieved, by using T significantly larger than τ. As a result, the detailed model has to be run for a fraction of the integration time only. The results of the previous section have shown that there is indeed a certain time-scale separation between the first dominant modes and higher-order modes (higher-order modes have higher fundamental frequencies), suggesting that a coarse time-stepping approach as described above is feasible.

The main limitation of the equation-free strategies is that although minimizing the use of the detailed model, the latter is run online. Here, thanks to the low dimensionality of the reduced basis considered, we propose to go one step further in the equation-free approach: instead of relying on detailed model simulations to estimate the $\dot{a}_m$ along the course of the dynamics (online), we explicitly determine the future values of the temporal coefficients, after a prescribed time horizon T, from their current values. In other words, denoting $\boldsymbol{a}(t) \in \mathbb{R}^M$ as the vector of temporal coefficients, we seek for the mapping that relates $\boldsymbol{a}(t)$ to $\boldsymbol{a}(t+T)$. We write this mapping as:

$$\boldsymbol{a}(t+T) = \mathscr{M}_T(\boldsymbol{a}(t)). \tag{14}$$

Clearly, the construction of such a mapping is an expensive task and an efficient approximation strategy is needed. Below, we propose to approximate the mapping $\mathscr{M}_T$ on a polynomial basis. The determination of the mapping being performed off-line, subsequent integrations of the dynamics is essentially cost-free. For instance,

$$\boldsymbol{a}(t+nT) = \mathscr{M}_T(\boldsymbol{a}(t+(n-1)T)) = \mathscr{M}_T \circ \mathscr{M}_T(\boldsymbol{a}(t+(n-2)T)) = \cdots$$

4.2. Polynomial approximation of the reduced system dynamics

In this paragraph, we focus on the polynomial approximation of the transformation $\mathscr{M}_T : \boldsymbol{a} \in \mathbb{R}^M \mapsto \mathscr{M}_T(\boldsymbol{a}) \in \mathbb{R}^M$ which expresses the increment in the reduced system's state variables after a time span T. We denote $Q_T(\boldsymbol{a})$ this polynomial approximation as:

$$Q_T(\boldsymbol{a}) \approx \mathscr{M}_T(\boldsymbol{a}). \tag{15}$$

Different strategies can be thought of to construct this approximation, for instance, through interpolation or fitting procedure. Here, we seek Q_T minimizing a mean-square distance ε_{Q_T} between Q_T and $\mathscr{M}_T$:

$$\varepsilon^2_{Q_T} = \int_{\mathbb{R}^M} (Q_T(\boldsymbol{a}) - \mathscr{M}_T(\boldsymbol{a}))^2 w_{\boldsymbol{a}}(\boldsymbol{a})\, \mathrm{d}\boldsymbol{a}, \tag{16}$$

DOI: 10.1002/fld

where $w_{\boldsymbol{a}} \geqslant 0$ is a normalized weight function. Since the coefficients a_m of the reduced system have variable amplitudes, it is convenient to rescale them by their respective eigenvalue $\sqrt{\lambda_m}$, i.e. to express the mapping in terms of the normalized A_m, hence,

$$\langle A_m \rangle_t = 0, \quad \langle A_i A_j \rangle_t = \delta_{i,j} \tag{17}$$

and Equation (16) can be recast as:

$$\varepsilon_{Q_T}^2 = \int_{\mathbb{R}^M} (Q_T(\boldsymbol{A}) - \mathscr{M}_T(\boldsymbol{A}))^2 w_{\boldsymbol{A}}(\boldsymbol{A}) \, \mathrm{d}\boldsymbol{A}. \tag{18}$$

The weight function $w_{\boldsymbol{A}}$ should ideally be selected as to minimize the error in the resulting dynamics of the reduced system. In fact, we only know that for the exact dynamics, the coefficients $A_m(t)$ have a unit variance and are uncorrelated but dependent. However, we have no information regarding the dependence structure of the coefficients $A_m(t)$ as it is emerging from the detailed flow model. Consequently, in the absence of further information, we shall consider, for simplicity, weight functions that are product form of a unique one-dimensional weight function $w(A_m)$:

$$w_{\boldsymbol{A}}(\boldsymbol{A}) = \prod_{m=1}^{M} w(A_m), \quad w(A) \geqslant 0, \quad \int_{\mathbb{R}} w(A) \, \mathrm{d}A = 1. \tag{19}$$

Now, let $\{p_i\}_{i=0}^{i=\infty}$ be the set of orthogonal polynomials with regard to the selected weight w,

$$\int_{\mathbb{R}} p_i(x) p_j(x) w(x) \, \mathrm{d}x = \| p_i \|_w^2 \delta_{i,j}, \tag{20}$$

where p_i is a polynomial with degree i, and let $\alpha = (\alpha_1 \ldots \alpha_M)$ be an integer multi-index. We define the multidimensional polynomials $p_\alpha(\boldsymbol{A})$ as:

$$p_\alpha(\boldsymbol{A}) = \prod_{m=1}^{M} p_{\alpha_m}(A_m). \tag{21}$$

The total degree of p_α is denoted as $|\alpha| = \sum_{m=1}^{M} \alpha_m$, and the polynomial approximation of the mapping is sought as

$$Q_T(\boldsymbol{A}) = \sum_{\alpha} (Q_T)_\alpha p_\alpha(\boldsymbol{A}), \tag{22}$$

where the $(Q_T)_\alpha \in \mathbb{R}^M$ are the coefficients of the polynomial approximation. In practice, the polynomial approximation has to be truncated to a finite degree denoted No, and ε_T^2 then defines an L_2-projection error (with regard to the inner product defined by $w_{\boldsymbol{A}}$) for the representation of the mapping on the truncated space spanned by the polynomials p_α, $|\alpha| \leqslant \mathrm{No}$. The dimension of the polynomial approximation space is therefore:

$$P + 1 = \frac{(\mathrm{No} + M)!}{\mathrm{No}! M!}. \tag{23}$$

Moreover, the polynomials p_α being orthogonal, the projection coefficients $(Q_T)_\alpha$ have for expressions:

$$(Q_T)_\alpha \| p_\alpha \|_w^2 = \int_{\mathbb{R}^M} \mathscr{M}_T(\boldsymbol{A}) p_\alpha(\boldsymbol{A}) w_{\boldsymbol{A}}(\boldsymbol{A}) \, \mathrm{d}\boldsymbol{A} \tag{24}$$

DOI: 10.1002/fld

where

$$\|p_\alpha\|_w^2 \equiv \int_{\mathbb{R}^M} p_\alpha^2(\boldsymbol{A}) w_{\boldsymbol{A}}(\boldsymbol{A})\,\mathrm{d}\boldsymbol{A}. \tag{25}$$

In other words, the determination of the approximation $Q_T(\boldsymbol{A})$ amounts to the evaluation of a total of $(P+1)$ M-dimensional integrals.

4.3. Practical determination of the polynomial mapping

In this paragraph, we provide details on the selection of the weight function w and numerical estimation of the integrals to yield the projection coefficients $(Q_T)_\alpha$.

4.3.1. Selection of the weight function. In this work, we choose the weight function that is the least informative with regard to the hypothesis on the evolutions of a coefficients $A(t)$, i.e. w maximizes the entropy $\mathscr{E}(w)$ defined as:

$$\mathscr{E}(w) \equiv -\int_{\mathbb{R}} w(A)\log w(A)\,\mathrm{d}A. \tag{26}$$

A first possibility is to base the weight function selection on the available information regarding the statistical characteristics of $A(t)$. We know, from the POD of the flow, that $A(t)$ has zero mean and unit variance, such that the maximization of $\mathscr{E}(w)$ is constrained by the two conditions (in addition to the normalization constraint in Equation (19)):

$$\int_{\mathbb{R}} A w(A)\,\mathrm{d}A = 0, \quad \int_{\mathbb{R}} A^2 w(A)\,\mathrm{d}A = 1 \tag{27}$$

and the maximum entropy principle yields:

$$w(A) = \frac{1}{\sqrt{2\pi}}\exp(-A^2/2). \tag{28}$$

For this weight function, the p_α are multi-dimensional Hermite polynomials.

However, we would like to apply the reduced model to situations which do not correspond to the flow dynamics analyzed for determining the POD, for instance, when perturbations (or control) are applied or during transients (see the results section below). In this case, constraints in Equation (27) may not hold anymore as the system may drift to a new asymptotic state, with different mean and variance for $A(t)$. In this case, it may be more relevant to simply assume that the evolution of a coefficient $A(t)$ remains in a finite interval, say $[-B,+B]$. Maximization of $\mathscr{E}(w)$ with $w(A\notin[-B,+B])=0$ and normalization constraint yield

$$w(A) = \begin{cases} 1/2B, & A\in[-B,+B], \\ 0, & A\notin[-B,+B]. \end{cases} \tag{29}$$

For this assumption, the p_α are multidimensional (rescaled) Legendre polynomials.

4.3.2. Computation of the projection coefficients. Determination of the projection coefficients $(Q_T)_\alpha$ involves the computation of M-dimensional integrals. Since M can be significantly large

DOI: 10.1002/fld

depending on the number of POD modes retained in the reduced basis, efficient numerical integration techniques are needed. Because the polynomials p_α and the weight functions $w_{\boldsymbol{A}}$ used in the following are classical ones, optimal quadrature formulas, namely Gauss quadratures [18], can be used. However, full tensorization of 1-D Gauss quadrature formulas suffers from the curse of dimensionality as M increases, such that the number of quadrature points, and so the number of detailed model resolutions, quickly becomes prohibitive. To maintain an acceptable number of simulations, we instead rely on sparse tensorization [19] to construct the M-dimensional quadrature formula. Specifically, integrals in Equation (24) are first transformed by appropriate change of variables to integrals over the unit hypercube $[0,1]^M$:

$$(Q_T)_\alpha = \frac{1}{\|p_\alpha\|_w^2} \int_{[0,1]^M} f_\alpha(\xi_1, \ldots, \xi_M)\, \mathrm{d}\xi_1 \ldots \mathrm{d}\xi_M. \tag{30}$$

With this change of integration variables, the integral is approximated by the cubature formula

$$\int_{[0,1]^M} f_\alpha(\xi_1, \ldots, \xi_M)\, \mathrm{d}\xi_1 \ldots \mathrm{d}\xi_M \approx \sum_{q=1}^{N_q} f_\alpha(\xi_1^{(q)}, \ldots, \xi_M^{(q)}) \tilde{w}^{(q)}, \tag{31}$$

where N_q, the number of cubature points, depends on the number of points in the one-dimensional formulas used for the construction and the requested accuracy for the integration [20]. Here, we have used the source code from [21] to generate the cubature points $\boldsymbol{\xi}^{(q)} = (\xi_1^{(q)} \ldots \xi_M^{(q)})$ and weights $\tilde{w}^{(q)}$ from embedded one-dimensional Féjèr quadrature formulas, which results in a number of cubature points

$$N_q = \mathcal{O}(2^l l^{M-1}), \tag{32}$$

where l is the polynomial degree of exactness for the cubature in Equation (31). Clearly, the evolution of the number of cubature points with l and M shows that the polynomial approximation of the mapping $\mathscr{M}_T$ will be feasible only for moderate M and l, i.e. if the mapping can be approximated using a low-order polynomial expansion, thus limiting *de facto* the time horizon T.

The derivation of the equation-free reduced model can be summarized as follows:

1. Construction of the reduced basis (see Section 3): **off-line**
2. Construction of the polynomial mapping: **off-line**
   For each of the N_q cubature points:
   (a) Integrate the detailed model between $t=0$ and $t=T$, with the initial condition as in Equation (13) with the values of the temporal coefficients $a_m^{(q)}(t=0)$ corresponding to the cubature points.
   (b) Projection of $\omega(\boldsymbol{x}, t=T)$ on the reduced basis to obtain the temporal coefficients $a_m^{(q)}(t=T)$.
   (c) Add weighted contribution of $a_m^{(q)}(t=T)$ to Q_T.
3. Initialize the temporal coefficients of the flow at $t=0$
4. While $t<nT$, repeat
   (a) Apply $\boldsymbol{a}(t+T) = Q_T(\boldsymbol{a}(t))$: **on-line**
   (b) $t \leftarrow t+T$
5. End

DOI: 10.1002/fld

Clearly, the most time-consuming part of the method is step 2, which is seen to be directly related to the number of cubature points (N_q) and coarse time-step T. We have not attempted to optimize this part of the method, but for large M, the use of more advanced techniques could be mandatory (e.g. adaptive sparse grid cubature or interpolation formulas, Quasi Monte Carlo integration, etc.). Note, again, that these computations are performed off-line and are embarrassingly straightforward to parallelize.

5. APPLICATION

The proposed model construction is applied to the flow around the cylinder at $Re=200$ and the POD basis introduced previously. The polynomial approximation of the mapping is performed in a pre-processing stage. Unless specified, the model involves the first 12 POD modes, the uniform weight function defined in Equation (29) with $B=2.8$ and a coarse time-step $T=0.2$ unit of time (roughly $\frac{1}{45}$ of the natural period of the flow). This value of T corresponds to a few tens of the detailed model time-step Δt. For the polynomial approximation of the mapping, unless explicitly stated, we set No$=5$ with a cubature formula having sufficient degree of accuracy, leading to $N_q \sim 47\,000$ cubature points. This fairly large number of simulations is performed in parallel and is done only once in a pre-processing stage.

5.1. Mapping

An illustration of the mapping (restricted to the plane $A_{m\geqslant 3}=0$ for convenience) is plotted in the left plot of Figure 6 as a 2-D vector field. Each vector corresponds to the displacement of the A_1 and A_2 coefficients over the coarse time-step, thus defining a vector in the (A_1, A_2)-plane. The limit-cycle (asymptotic trajectory, see below) for the detailed model is also plotted for comparison. Although difficult to appreciate from the figure, the trajectory is divergent inside the limit-cycle while it is convergent in the outer region, leading to trajectories for the mapping integration that

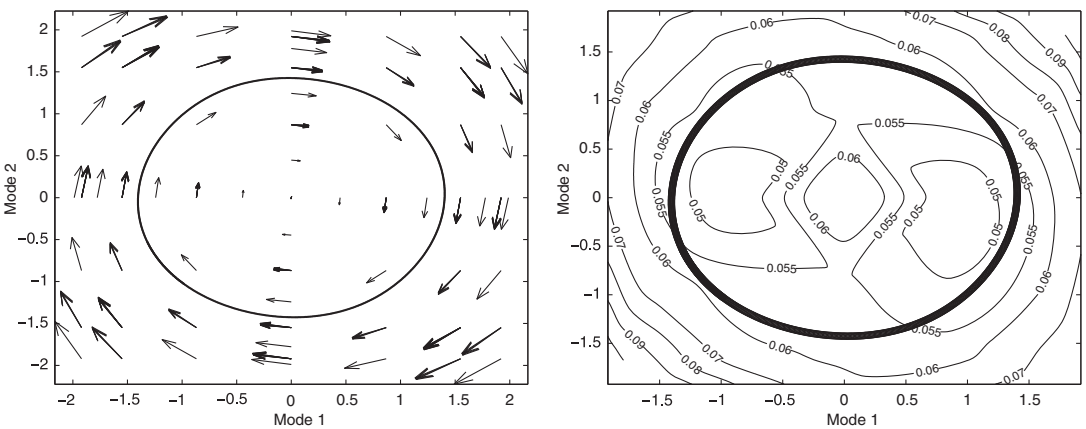

Figure 6. Left: view of the mapping in the $A_{m\geqslant 3}=0$ plane. Right: corresponding polynomial approximation error E_Q. The in-plane limit-cycle of the detailed model is also plotted for comparison (thick solid line). $M=12$, $T=0.2$, No$=5$.

DOI: 10.1002/fld

tends to the detailed model limit-cycle as discussed below. The right plot in Figure 6 shows the approximation error using Q_T instead of the actual mapping $\mathscr{M}_T$, in the $A_{m\geqslant 3}=0$-plane. Plotted is the local error ε_Q defined as:

$$E_Q^2(\boldsymbol{A}) \equiv \frac{\|\mathscr{M}_T(\boldsymbol{A}) - Q_T(\boldsymbol{A})\|^2}{\|\mathscr{M}_T(\boldsymbol{A})\|^2}. \tag{33}$$

While the plots in Figure 6 are restricted to a 2-D plane, the error E_Q is seen to be essentially uniform over the domain, as one may have anticipated from using the uniform weight function. This fact directly implies that the present mapping strategy is not restricted to the immediate vicinity of the natural cycle limit but extends over the whole domain of the reduced model investigated, namely here, $A_m \in [-B, +B]$.

5.2. *Asymptotic dynamics*

The accuracy of the reduced model dynamics is first assessed. To this end, the trajectory of the reduced system, obtained by successive applications of the polynomial mapping, is compared with the projection on the reduced basis of the detailed model solution (i.e. by directly solving the full set of Navier–Stokes equations as discussed in Section 2).

5.2.1. Trajectory of the reduced system. The flow is initialized by setting all POD coefficients to zero, except A_0 which is set to 1: i.e. the initial state corresponds to the mean flow field. The polynomial mapping is then iteratively applied to obtain a succession of coordinates corresponding to the phase portraits reported in Figure 7 for the first most energetic modes. After each time-horizon, the state of the model is represented as a dot in the phase space (here we only plot the first four phase portraits). It is seen that the system undergoes a transient dynamics (to be discussed later in Section 5.3) and later reaches an asymptotic state. The asymptotic trajectory defines a limit-cycle showing that the mapping destabilizes the flow from its initial mean state and drives the reduced model to its unsteady attractor. The reduced model limit-cycle is seen to compare well with the detailed model one. Specifically, the distance between the detailed and reduced model phase portraits is however increasing with the mode index, denoting an effect of the basis truncation, but the agreement for the first modes is excellent.

This good agreement between the detailed model and the polynomial mapping limit-cycles shows that the flow obtained through the reduced model and the mapping iterations obeys a dynamics close to the detailed one. In fact, not only the asymptotic limit-cycle is in close agreement, but the frequency spectra of the first modes also compare favorably to the spectra from the detailed model in the asymptotic region (not shown).

It is to be noted that the asymptotic state obtained with the present reduced model is stable: no drift is reported after as many as thousands of vortex shedding periods. This is due to the fact that the mapping expresses the evolution of the POD coefficients over a coarse time-step as predicted by the *detailed model*. Consequently, no approximation is made *during* the path of the coefficients within a coarse time-step T, and the truncation errors due to both the finite number of modes in the reduced basis and the polynomial approximation of the mapping do not build up as time advances; instead the trajectory is continuously driven by the mapping toward the asymptotic limit-cycle of the detailed model, provided that the polynomial mapping error remains low compared with the contraction rate of the dynamics toward the detailed flow attractor. In fact, the only source of error in the integration scheme comes with the initialization of the flow with its Mth-order

DOI: 10.1002/fld

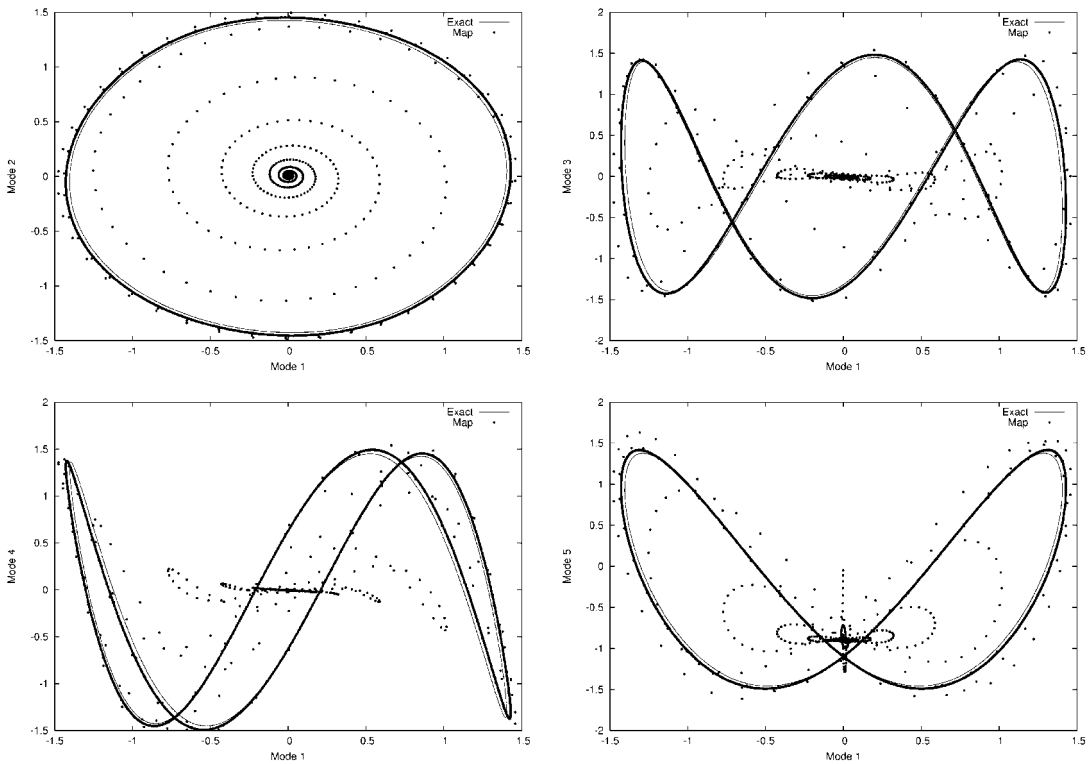

Figure 7. Phase portraits: A_2–A_5 as functions of A_1 from the initial state $A_m(t=0)=\delta_{m,0}$ for the polynomial mapping (dots). The trajectory of the reduced model (dots) is an expanding spiral from the origin toward the asymptotic attractor. Also plotted for comparison are the asymptotic phase portraits of the detailed model (solid lines). $M=12$, $T=0.2$, No$=5$.

representation at the start of the coarse time-step. We have verified that the initialization with, in addition to the Mth-order truncation, some non-zero modes of indexes $>M$ (randomly set) does not affect the mapping provided that T is large enough and the energy of the added modes is not too large, as expected from the scale-separation assumption.

The resulting stable model is in contrast with the Galerkin techniques where the projection of the system equations onto the reduced model modes suffers from truncations errors, which drift the solution off with time. This is a major problem and several techniques have been proposed to improve the method, for instance, using spectral viscosities [5], using a non-linear Galerkin projection [3], a norm in the Sobolev space H^1 to account for both the basis functions and the derivatives of the snapshots (see [4]) or introducing additional terms in the Galerkin formulation, calibrated through an optimization procedure [6–8]. In contrast to these, the equation-free strategy is intrinsically stable and does not require special treatments to ensure the stability of the trajectory.

5.2.2. Influence of the polynomial mapping parameters. The relevance and impact of the selected weight function $w_{\boldsymbol{A}}$ are now investigated. The comparison is made on the asymptotic trajectories for the polynomial mappings determined using the constant weight function in Equation (29) and

DOI: 10.1002/fld

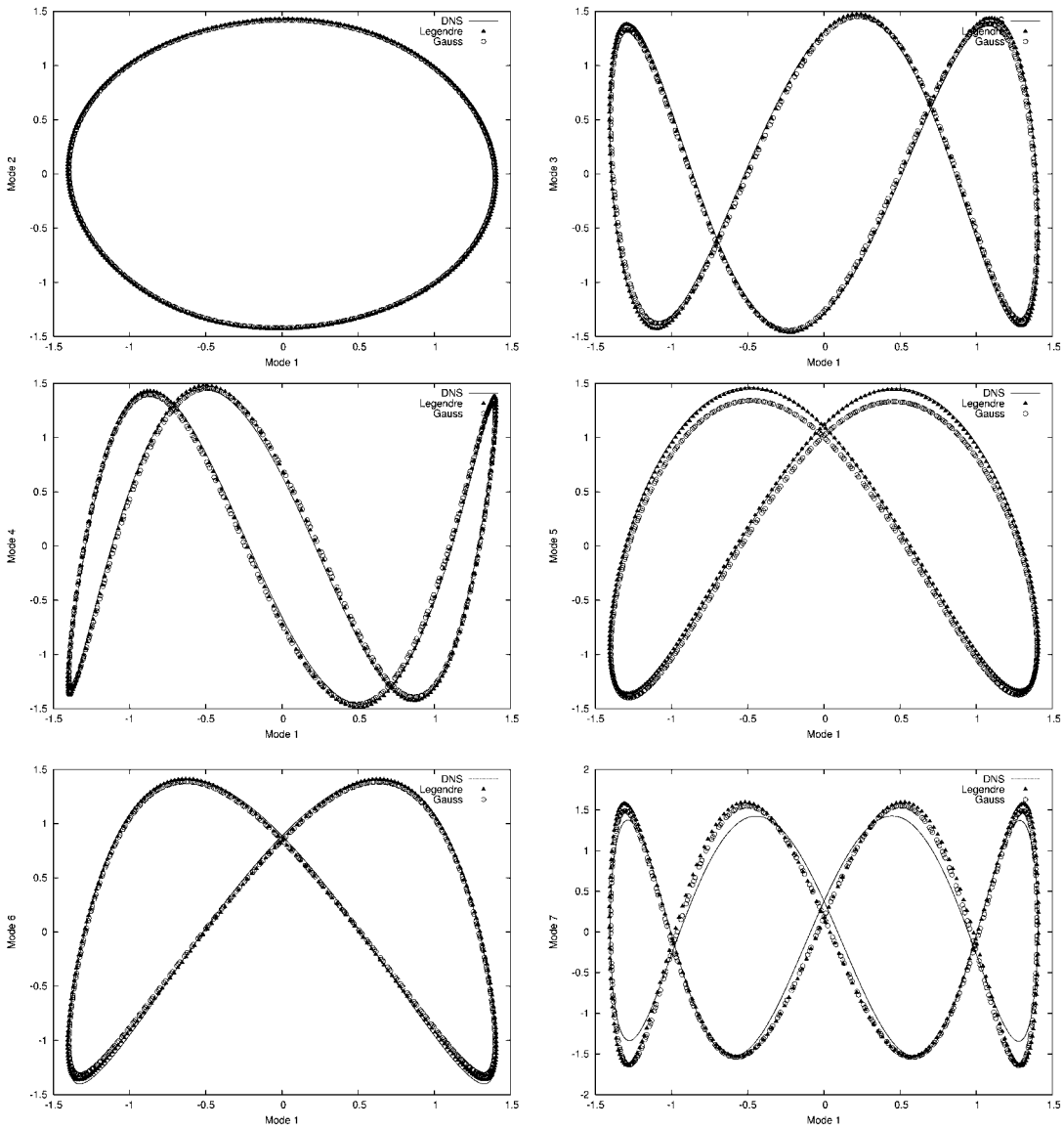

Figure 8. Comparison of the phase portraits, $A_2(t)$ to $A_5(t)$ as functions of $A_1(t)$, using constant (Equation (29)) and Gaussian (Equation (28)) weight functions. Also reported for comparison are the phase portraits for the detailed model (labelled DNS). $M=12$, $T=0.2$ and $\mathrm{No}=5$.

the Gaussian weight function in Equation (28). The corresponding phase-portraits are reported in Figure 8, together with the detailed model reference. It is clear that the agreement with the detailed model is good for both weight functions, and no clear advantage is seen in terms of accuracy. The selection of the weight functions is thus not a critical one, at least as long as the order No for the polynomials approximation is high enough and provided that the trajectory remains in the mapping bounds

DOI: 10.1002/fld

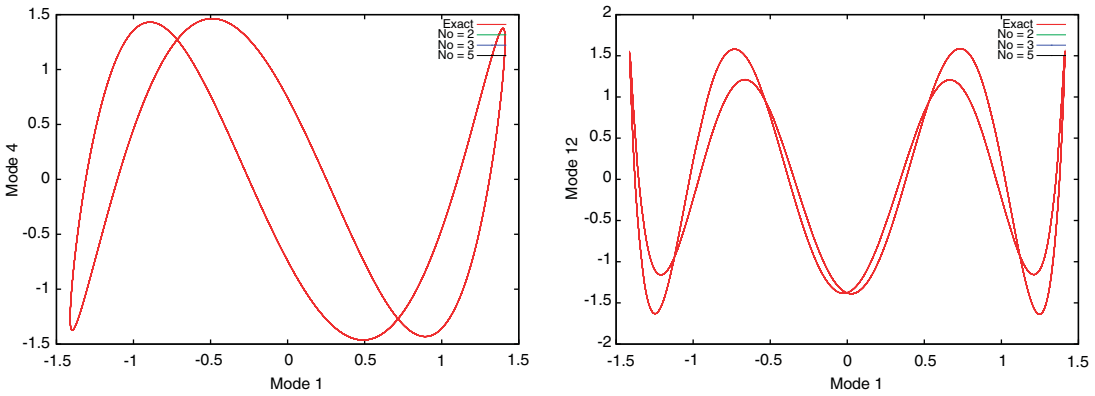

Figure 9. Asymptotic phase portraits of A_4 (left) and A_{12} (right) as a function of A_1 for different polynomial approximation order No of the mapping. $T=0.2$.

$(A_m(t)\in[-B,+B])$ for the constant weight function. From this perspective, the Gaussian weight function may appear more appropriate when one cannot bound the temporal coefficients evolution *a priori*.

The mapping process basically consists in a polynomial approximation of the evolution of the POD modes coefficients over a coarse time-step T, hence, the accuracy of the approximation is directly related to the polynomial order No. The influence of No is investigated in Figure 9, where the phase portrait A_4 and A_{12} as a function of A_1 are plotted for different polynomial orders. The exact phase portrait given by the detailed model is also plotted for comparison. Note that for all No, the same cubature formula ($l=5$) was used for the evaluation of the multidimensional integrals involved in the determination of Q_T. As the polynomial order increases, the agreement is seen to improve as the evolution of the POD coefficient over the coarse time-step is better approximated. In fact, the selection of an appropriate polynomial order No essentially depends on the characteristic time-scales of the modes in the reduced basis: when including in the reduced basis modes with higher index (faster time scales), the mapping to be approximated becomes more and more complex, thus requiring higher No for a fixed coarse time-step T. This is clearly demonstrated by comparing the phase portraits for A_4 (left) and A_{12} (right): for No$=3$, the approximation of the exact phase portrait is fairly good for A_4, whereas it is rather poor for A_{12}. This observation also suggests future improvement of the method where variable appropriate polynomial orders are used for different A_m. It would allow for a significant reduction of the number of cubature points. Further increasing the polynomial order hardly improves the approximation for A_4 whereas it has a strong effect for A_{12}.

As just discussed above, for a given coarse time-step T, the higher the order No, the better the approximation of $\mathscr{M}_T$ by Q_T. In a dual way, for a fixed polynomial order No, a lower T leads to smaller and smoother variations of the POD coefficients over a coarse time-step, and thus more easily accountable maps with a low polynomial order: one can expect the polynomial approximation error to decrease as T decreases. On the other hand, the reduced simulation is, by essence, a truncated representation of the flow and only a limited number of modes is accounted for when initializing the detailed model. For short coarse time-steps, the truncated modes do not have enough time to fully develop in the detailed model simulation step, leading to mappings $\mathscr{M}_T$

DOI: 10.1002/fld

that are less and less representative of the actual system's dynamics as T decreases. One finally ends up with two opposite trends: a small T allows for accurate polynomial approximation of the mapping but introduces a sort of cut-off frequency in the flow dynamics, whereas a large T improves the reduced system dynamics but raises the problem of the polynomial approximation accuracy. Thus there exists an optimum balancing those two phenomena and achieving the best reduced model. This has been verified in our numerical experiments, using a fixed polynomial order No$=5$ and variable coarse time-step T: the optimum was found for $T\simeq 0.3$, the error on the dynamics increasing as T is further increased and the method eventually becomes unstable for $T>0.8$ (not shown): increasing No would be necessary to ensure the stability. As a closing remark on the selection of the polynomial mapping parameters, we point out that the computational cost of the mapping determination increases linearly with T and exponentially with No, while the application of the mapping is essentially inexpensive.

5.2.3. Convergence with the number of modes M. The impact of the dimension of the reduced basis on the reduced model dynamics is now considered. To this end, we define E_Ω as

$$E_\Omega^2 \equiv \left\langle \frac{\int (\omega' - \Omega')^2 \, \mathrm{d}\boldsymbol{x}}{\int \omega'^2 \mathrm{d}\boldsymbol{x}} \right\rangle_t , \tag{34}$$

where the $'$ symbol denotes the fluctuating part of a quantity.

Here the time average is restricted to the asymptotic state, the transient stage being disregarded. The decay of the error in the dynamics, as measured by E_Ω, when M is increased is shown in Figure 10. For low M, the detailed dynamics is poorly captured as the dimension of the parameters space is too small to fully develop the attractor; this results in a large error $E_\Omega>1$. Indeed, the chosen embedding dimension of the system attractor should be large enough so that its dynamics is deterministic, i.e. that there exists a bijective operator between the time and the state vector over a period of the reduced system. In other words, the trajectory of the system should never cross itself. Dynamical system theory shows that a minimum subspace dimension exists so that

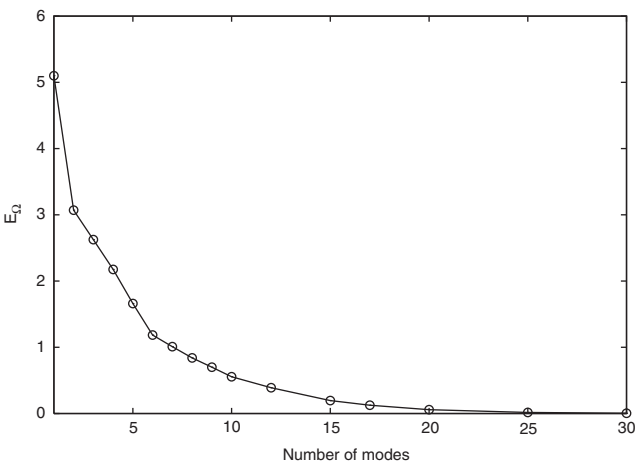

Figure 10. Error E_Ω (see Equation (34)) as a function of the reduced basis dimension. $T=0.15$.

DOI: 10.1002/fld

the system projection onto that subspace obeys this condition (see [22–24]). For larger M, the error decreases as more and more components are introduced in the basis.

5.3. Transient dynamics

So far, the results have been presented for the asymptotic state of a fully developed Kármán vortex street behind the cylinder which has served for the construction of the reduced basis. It is also of interest to focus onto the dynamics in transient state and to investigate the range of validity of the reduced model. This is typical of what happens when a control is applied to the flow which then transits towards a new attractor. Being able to reproduce these driven dynamics are then of critical importance. In contrast with most other methods (regression-based), this is intrinsically achieved in the present equation-free technique which does not rely on approximating the system along its attractor but rather on a whole domain of the state space, as prescribed by the weight function.

Starting from all POD coefficients $A_{m>0}$ set to zero (time-averaged field), the temporal developments of the flow for the detailed model and the mapping iterations are compared in Figure 11 as the time evolution of the amplitudes of coefficients A_1 and A_3. The instantaneous amplitudes of the coefficients are computed by means of Hilbert's transform. Starting from zero, the amplitudes of A_1 and A_3 then grow and finally reach comparable asymptotic values. However, while the flow does eventually converge to the correct asymptotic attractor, as extensively discussed above, the reduced model ($M=10$) leads to a significantly delayed development of the flow compared with the detailed model. This delayed destabilization of the reduced flow can be explained by the low dimensionality of the reduced basis. Indeed, the initial growth phase is driven by the amplification of small perturbations of the unstable mean flow including small and localized flow structures which are poorly accounted for in the reduced model. As a result, the growth rate of these instability modes is affected, making the energy growth in the large scales to be delayed in the reduced model. In fact, in the transient stage where the actual wake is only partially developed, the reduced basis representation is poor as it has been constructed from snapshots of a fully developed wake. However, once a minimal amount of energy is carried by the large-scale modes, the flow time scale is driven by large structures and the growth rate of low mode indexes is seen to be similar for

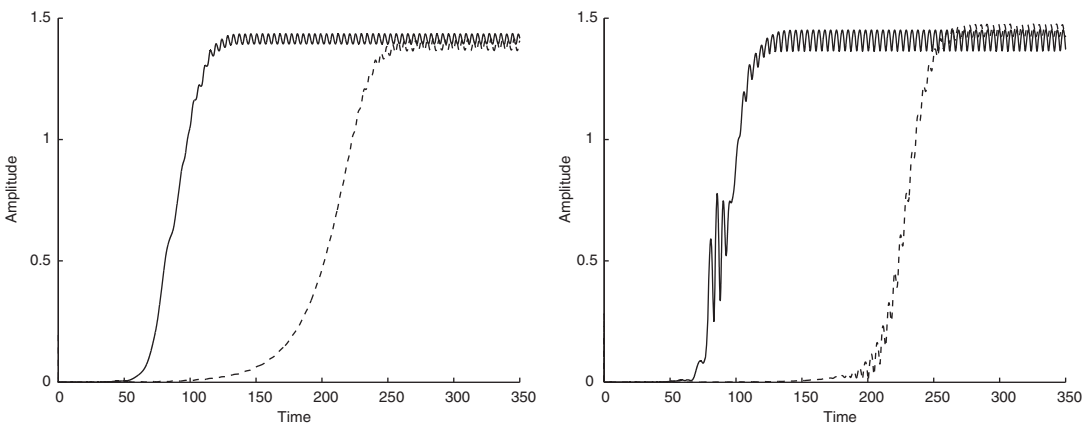

Figure 11. Instantaneous amplitude of $A_1(t)$ (left) and $A_3(t)$ (right) for the reduced model (dashed line) and detailed model (solid line). $T=0.2$, No$=5$, $M=10$.

DOI: 10.1002/fld

both the detailed and reduced models. This experiment shows that, in addition to an appropriate equation-free strategy, it is also necessary to consider robust reduced bases that can accurately account for a wide range of system conditions. This is particularly crucial in view of using the reduced model for system control. The issue of deriving a robust reduced basis and application of the equation-free reduced model to control problems was considered in [25].

6. CONCLUSION

This paper has presented a computationally efficient technique for model reduction of complex physical systems. The reduced model is established in two stages. First, a low-dimensional reduced basis is constructed by a suitable projection of the system state involving a large number of degrees of freedom. The reduced basis is meant to preserve the essential features of the original system. Different strategies can be used for this task, and we have selected here the classical proper orthogonal decomposition (or Karhunen-Loève expansion), which is performed in practice using the snapshots method. Second, a reduced model giving the time-evolutions of the system's projection coefficients on the reduced basis is constructed. The main characteristic of the proposed reduced model is its equation-free character: the time-integration does not involve the resolution of a set of differential equations, as for classical methods, but instead relies on an explicit transformation (a mapping) of the coefficients during a coarse integration time-step. The mapping is computed once for all in a pre-processing stage using the detailed model, and stored as an approximated polynomial transformation for subsequent use. The procedure results in an efficient reduced model, where the time-integration of the reduced model amounts to successive application of a low-cost polynomial transformation.

The effectiveness of the proposed reduced model is demonstrated for the problem of a two-dimensional flow around a circular cylinder at $Re = 200$. Prediction of the reduced model is compared with the detailed model which involves the resolution of a large set of coupled set of equations involving 180×180 degrees of freedom. In contrast, a typical dimension for the reduced model is $M = 12$. It is shown that the reduced model can accurately represent the asymptotic dynamics of the detailed model used for its construction. In particular, the reduced model does not suffer from the unstable character of Galerkin-based reduced models which drift in time due to unresolved small scales. Here, provided that the mapping is sufficiently well approximated, the simulation is intrinsically stable and the error resulting from the model reduction remains constant in time, even after thousands of vortex shedding periods. Further, in contrast with other regression-based methods employed to determine the reduced model equations coefficients, the present approach establishes a reduced model valid over a prescribed domain of the state space spanned by the reduced basis.

Therefore, the validity of the model is not restricted to dynamics in the immediate vicinity of the system's asymptotic state, provided that the reduced basis remains valid to account for different dynamics. This robustness is of particular interest in view of controlling the system as its trajectory in the phase space would then depart from the one the coefficients regression was determined from. The whole reduction-control strategy was investigated in [25] to demonstrate the suitability of the present method for the control of complex systems.

In terms of computational complexity, the mapping construction in the current implementation requires multiple off-line time-integration of the detailed model to evaluate M-dimensional integrals. This is clearly a limitation as M increases due to the curse of dimensionality of the

DOI: 10.1002/fld

integration rules used. For better efficiency and problems with larger M, one should consider more advanced integration techniques such as adapted sparse grid cubature rules.

REFERENCES

1. Sagaut P. Large eddy simulation for incompressible flows. *Scientific Computation* (3rd edn). Springer: Berlin, 2006.
2. Lam SH, Goussis DA. The CSP method for simplifying kinetics. *International Journal of Chemical Kinetics* 1994; **26**:461–486.
3. Marion M, Temam R. Nonlinear Galerkin methods. *SIAM Journal on Numerical Analysis* 1989; **26**:1139–1157.
4. Iollo A, Lanteri S, Désidéri J-A. Stability properties of POD-Galerkin approximations for the compressible Navier–Stokes equations. *Theoretical and Computational Fluid Dynamics* 2000; **13**:377–396.
5. Sirisup S, Karniadakis GE. A spectral viscosity method for correcting the long-term behavior of POD models. *Journal of Computational Physics* 2004; **194**:92–116.
6. Galletti B, Bottaro A, Bruneau C-H, Iollo A. Accurate model reduction of transient and forced wakes. *European Journal of Mechanics B/Fluids* 2007; **26**(3):354–366.
7. Cordier L, Abou El Majd B, Favier J. Calibration of POD Reduced-Order Models using Tikhonov regularization. *International Journal for Numerical Methods in Fluids* 2009; DOI: 10.1002/fld.2074.
8. Bergmann M, Bruneau C-H, Iollo A. Enablers for robust POD models. *Journal of Computational Physics* 2009; **228**:516–538.
9. Lorang Vodinh L, Podvin B, Le Quéré P. Flow estimation using neural network. *Turbulence and Shear Flow Phenomena*, Williamsburg, VA, U.S.A., 27 June 2005.
10. Vanel JM, Peyret R, Bontoux P. A pseudospectral solution of vorticity-streamfunction equations using the influence matrix technique. In *Numerical Methods for Fluid Dynamics*, Morton KW, Baines MJ (eds). Clarendon Press: Oxford, 1986; 463–475.
11. Daube O. Resolution of the 2D Navier–Stokes equations in velocity–vorticity form by means of an influence matrix technique. *Journal of Computational Physics* 1992; **103**:402–414.
12. LeMaître OP, Scanlan RH, Knio OM. Estimation of the flutter derivatives of an NACA airfoil by means of Navier–Stokes simulation. *Journal of Fluids and Structures* 2003; **17**:1–28.
13. Lumley JL. The structure of inhomogenous turbulent flows. In *Atmospheric Turbulence and Radio Propagation*, Yaglom AM, Tatarski VI (eds). Nauka: Moscow, 1967; 166–178.
14. Holmes P, Lumley JL, Berkooz G. *Turbulence*, *Coherent Structures*, *Dynamical Systems and Symmetry*. Cambridge University Press: Cambridge, 1996.
15. Sirovich L. Turbulence and the dynamics of coherent structures. Part 1: coherent structures. *Quaterly of Applied Mathematics* 1987; **45**(3):561–571.
16. Rico-Martínez R. Gear CW, Kevrekidis IG. Coarse projective kMC integration: forward/reverse initial and boundary value problems. *Journal of Computational Physics* 2004; **196**(2):474–489.
17. Kevrekidis IG, Gear CW, Hyman JM, Kevrekidis PG, Runborg O, Theodoropoulos K. Equation-free multiscale computation: enabling microscopic simulators to perform system-level tasks. *Communications in Mathematical Sciences* 2003; **4**:715–761.
18. Abramowitz M, Stegun IA. *Handbook of Mathematical Functions*. Dover: New York, 1970.
19. Smolyak SA. Quadrature and interpolation formulas for tensor products of certain classes of functions. *Doklady Akademii Nauk SSSR* 1963; **4**:240–243.
20. Petras K. Fast calculation of coefficients in the Smolyak algorithm. *Numerical Algorithms* 2001; **26**:93–109.
21. Petras K. Asymptoticaly minimal Smolyak cubature. Preprint. Software available at: http://www-public.tu-bs.de:8080/~petras/software.html.
22. Takens F. *Detecting Strange Attractors in Turbulence*. Lecture Notes in Mathematics, vol. 898. Springer: New York, 1981; 366–381.
23. Gibson JF, Farmer JD, Casdagli M, Eubank S. An analytic approach to practical state space reconstruction. *Physica D* 1992; **57**(1–2):1–30.
24. Broomhead DS, King GP. Extracting qualitative dynamics from experimental data. *Physica D* 1986; **20**(2–3): 217–236.
25. Mathelin L, Le Maître OP. Robust model reduction and control of the flow past a circular cylinder with uncertainty. *Computers and Fluids* 2008; **38**(6):1168–1182.